# PROCESS SIMULATION AND OPTIMISATION OF $H_2$ PRODUCTION FROM ETHANOL STEAM REFORMING AND ITS USE IN FUEL CELLS.

## 1. Thermodynamic and kinetic analysis.

Ilenia Rossetti* , Matteo Compagnoni and Mauro Torli

Dip. Chimica, Università degli Studi di Milano, INSTM Unit Milano-Università and CNR-ISTM, via Golgi 19, 20133 Milano, Italy

**ABSTRACT**

Ethanol was considered as raw material for hydrogen production by steam reforming. Reformate purification from CO to feed fuel cells may be accomplished by well established routes, such as high and low temperature water gas shift and methanation, to be integrated with the $H_2$ production unit. A PEM fuel cell can be used for power cogeneration. Data and layout have been inspired by an existing unit Helbio, GH2 -BE- 5000, capable of delivering 5 $kW_{electrical}$ + 5 $kW_{thermal}$ output.

In order to size and simulate the steam reforming reactor, reliable and complete kinetic data are needed. Partial information has been only found in the literature, in spite of well detailed analysis of the reaction mechanism. In the first part of this work, alternative reaction networks and kinetic models are critically reviewed and compared. Reliable and complete models were applied to literature data to estimate sound kinetic parameters for reactor modeling and simulation, objective of the second part of this work.

* Corresponding author: fax 0039-02-50314300; email ilenia.rossetti@unimi.it

At first, the equilibrium composition of a reacting mixture was calculated as a function of temperature, pressure and water/ethanol ratio, to define the boundary conditions of this investigation. Then, after selection of three alternative models to represent the complex reaction scheme of bioethanol steam reforming, a full set of kinetic parameters has been estimated and checked for consistency. The latter has been successfully applied to reformer sizing and simulation, as fully described in *part 2*.

*Keywords:* Ethanol steam reforming; Process simulation; $H_2$ production; Fuel cells; Kinetic modeling.

## 1 - INTRODUCTION

The global energy system is still mostly based on fossil fuels. The use of these resources is inextricably linked to the emission of $CO_2$ in the atmosphere and often accompanied by other pollutants. In this perspective, the introduction of an energy carrier, easily obtainable from renewable sources by means of large-scale and highly efficient processes, then used to produce energy at decentralized level without emission of pollutants, would break down the local environmental impact of fuels and reduce the global warming.

There are two main disadvantages in using any energy carrier that is not a primary source. The first is the net energy loss that occurs during the transformation from one form of energy to another. Furthermore, every transformation involves a process and an additional facility in the chain, hence, ultimately, an increase of the unit cost of energy. The loss that occurs using an intermediate energy vector certainly represents a worsening of the overall performance, but this may be limited, canceled or even improved, if the carrier allows the production of energy in downstream processes with higher yields than those achievable with

the starting source. This may be the case of $H_2$, which can be fed to fuel cells allowing the production of electricity, a valuable form of energy, with an excellent yield, together with the cogeneration of thermal energy.

Being $H_2$ mostly produced from fossil sources, it is more expensive than traditional fuels, and therefore its use in internal combustion engines is not economically feasible. However, the introduction of a specific market for fuel cells has witnessed a growth of interest for this energy vector. In this context, the use of renewable resources for the production of $H_2$ should be carefully analysed to assess not only its environmental sustainability through life-cycle analysis (LCA), but also its economical feasibility.

The use of biofuels, *e.g*. bioethanol and biodiesel, in the transportation sector has undergone a significant increase over the last decade thanks to favorable energy policies in several countries. Considering the mature technology of existing processes for the reforming of hydrocarbons, the implementation of similar processes with other substrates, such as alcohols, appears natural. The use of ethanol for this purpose represents an opportunity to produce $H_2$ from renewable sources [1].

Today, bioethanol takes the widest slice of the production of biofuels worldwide. It is derived from the fermentation of polysaccharides, obtained from the processing of certain agricultural products, today almost exclusively from sugar cane and corn. The largest producers of these crops are, respectively, Brazil and the USA. A calculation of the energy retained in ethanol compared to that contained in the original glucose shows that 97.5% of the energy associated with the glucose is recovered. The distillation of the aqueous solution obtained by fermentation produces the 96 vol% azeotrope, which can be further dehydrated by adsorption on molecular sieves. Such hard dehydration is compulsory if ethanol is thought as additive for gasoline, but it can be avoided if it is used as substrate for steam reforming, at least in principle.

Sugar cane, corn and other agricultural products poor in starch, can be converted into ethanol and the technologies of these processes are mature and easy to spread. However, the cost of ethanol produced in this way is quite high, mainly because the crops used are also intended for food and feed purposes, also raising ethical issues. Waste from wood processing and the production and recycling of paper, agricultural and forestry residues, or crops specifically dedicated are among the constituents of lignocellulosic biomass. Recently, ethanol production from this source is gaining considerable interest, as testified by the construction of a semi-commercial plant (40 kton/year), first in the world, for the production of bioethanol from lignocellulosic feedstocks by the Mossi&Ghisolfi group [2].

For the steam reforming of ethanol (SRE), the most important process variable, besides temperature, is the $H_2O/C_2H_5OH$ feeding ratio. Its increase strongly inhibits the deposition of coke and it reduces the equilibrium fractions of CO and $CH_4$ in favor of $H_2$ and $CO_2$. Apart from a few publications based on an Eley Rideal type mechanism for SRE [3], $H_2O$ or hydroxyl species are competitive with ethanol for adsorption. Hence, the increase of the $H_2O/C_2H_5OH$ feeding ratio above a certain optimal value may even cause a decrease in the reaction rate [4]. The optimal ratio $H_2O/C_2H_5OH$ should be carefully evaluated also from an economic point of view. A higher content of $H_2O$ in the bioethanol fed leads to an appreciably lower cost of the solution. Commercial 50% solutions may be available at lower cost that the azeotrope ones [5,6]. On the other hand, too diluted solutions require surplus energy for the evaporation of $H_2O$ in excess and it may affect also the design of the energy recovery system [7]. Therefore, this parameter will be specifically taken into account in the following.

In the present work, we considered a possible unit for the distributed electrical and thermal cogeneration of energy starting from bioethanol, for a stationary residential target. A unit constituted by different reactors connected in series for $H_2$ production and purification (by water gas shift and methanation) and a PEM fuel cell has been considered. Process simulation needs reliable and complete kinetic and thermodynamic parameters, which are

not really easy to find in the literature. Therefore, we first focused on the identification of thermodynamic and kinetic models suitable for the description of each reactor, objective of this first part of the paper. Then, after the set up and simulation of a flowsheet representing an existing demonstrative unit present in our facilities [8], we optimised heat recovery between different streams in order to improve process efficiency (part 2). We specifically focused on the effect of ethanol/water feeding ratio. Indeed, as recalled above, this is a very important topic determining the cost of the feedstock (less purified ethanol may be used for this application, provided that it is used on-site or that its transportation costs per energy density are sustainable) and thus the overall energy production cost.

## 2 – MODELS AND METHODS

The steam reforming of ethanol follows the ideal stoichiometry:

$$CH_3CH_2OH + 3H_2O \rightarrow 6H_2 + 3CO_2 \quad \text{(R1)}$$

$\Delta_rH^0$=173.4 kJ mol$^{-1}$ when considering the reactants in gas phase, $\Delta_rH^0$=347.4 kJ mol$^{-1}$ in liquid phase. It has a high value of the equilibrium constant already above 600 K [1], however, going through the most elementary steps, it is plausible the formation of other products. Indeed, the most likely reactions for $C_2H_5OH$ during SRE are the following [4,9].

The formation of syngas:

$$CH_3CH_2OH + H_2O \rightarrow 2CO + 4H_2 \quad \text{(R2)}$$

Ethanol decomposition to form $CH_4$:

$$CH_3CH_2OH \rightarrow CH_4 + CO + H_2 \quad \text{(R3)}$$

$$CH_3CH_2OH + H_2O \rightarrow CH_4 + CO_2 + 2H_2 \quad \text{(R4)}$$

Dehydrogenation of ethanol to acetaldehyde:

$$CH_3CH_2OH \rightarrow CH_3CHO + H_2 \quad \text{(R5)}$$

Condensation of ethanol to acetone:

$$2CH_3CH_2OH \rightarrow CH_3COCH_3 + CO + 3H_2 \quad \text{(R6)}$$

Acetaldehyde and acetone are found especially during testing at low temperature and high space velocity (GHSV), *i.e.* at low conversion. However, under appropriate operating conditions such intermediates can be completely converted into other thermodynamically stable products, through acetaldehyde decarbonilation and steam reforming of both the aldehyde and ketone [10,11].

$$CH_3CHO \rightarrow CH_4 + CO \quad \text{(R7)}$$

$$CH_3CHO + H_2O \rightarrow 2CO + 3H_2 \quad \text{(R8)}$$

$$CH_3COCH_3 + 2H_2O \rightarrow 3CO + 5H_2 \quad \text{(R9)}$$

Additionally methane steam reforming (SRM) and the water-gas shift reaction (WGS) may occur.

$$CH_4 + H_2O \leftrightarrows CO + 3H_2 \quad \text{(R10)}$$

$$CO + H_2O \leftrightarrows CO_2 + H_2 \quad \text{(R11)}$$

These two reactions are reversible. In particular, the SRM is favored by high temperature, the WGS is favored at low temperature. Therefore, ideally, the catalyst should promote as much as possible SRE at low temperature, in order to improve $H_2$ yield through WGS, and inhibit CO methanation, also favored at low temperature. Alternatively, at high temperature the reverse WGS reaction may take place [12].

Among the possible reactions for $CH_4$ the following has been also proposed [4,13]:

$$CH_4 + 2H_2O \leftrightarrows CO_2 + 4H_2 \quad \text{(R12)}$$

Its reverse, the methanation of $CO_2$, is supposed to take place at low temperature, causing a reduction in efficiency [14].

Carbon is one of the components with a certain thermodynamic stability under the SRE operating conditions and may induce catalyst deactivation. Among the processes that lead to its deposition, definitely the fastest is ethanol dehydration leading to ethylene. The olefin may then undergo dehydrocyclisation condensations leading to the formation of amorphous carbon.

$$CH_3CH_2OH \leftrightarrows CH_2CH_2 + H_2O \quad \text{(R13)}$$

$$nCH_2CH_2 \rightarrow \text{coke} + 2nH_2 \quad \text{(R14)}$$

It is known that not only the dehydration of ethanol, but practically all stages of the sequence above are catalyzed by acid sites. For this reason, among the simplest solutions to inhibit the deposition of coke, the use of alkaline promoters has been largely explored [15,16]. Some other researchers suggest to operate the SRE in two series reactors, the first operating with a catalyst for the dehydrogenation of ethanol to acetaldehyde, the second for the steam reforming of the latter, which has a lower propensity to form coke [10,17]. Other reactions affecting carbon formation are the Bouduard reaction, the gasification of coal and the decomposition of $CH_4$.

$$CO_2 + C \leftrightarrows 2CO \quad \text{(R15)}$$

$$C + H_2O \leftrightarrows CO + H_2 \quad \text{(R16)}$$

$$CH_4 \leftrightarrows C + 2H_2 \quad \text{(R17)}$$

All of them are reversible reactions and they are written in the sense in which they are favored by increasing temperature. Therefore, the first two are responsible for the deposition of coke at low temperature, on the contrary the third is considered responsible for its formation at temperature exceeding 700 K [1]. In a thermodynamic study on the SRE process [3], three forms of carbon were considered: graphite, amorphous and multi-walled carbon nanotubes (MWCNTs). Graphite is the most stable phase at low temperatures, while over 400°C, the MWCNTs are the main constituent of the deposits, as extensively reported in the literature for Co and Ni-based catalysts [18-22]. Nevertheless, amorphous carbon, although the less stable form, is the one most frequently found on a practical level, because the pathways leading to its formation are much faster.

The expected products distribution depends of course on the reaction conditions, but also on feed composition, *e.g*. on the presence of inert gases [17,23,24]. Different $H_2$ purification stages should follow the steam reforming reactor based on this, such as a “reacting route”, based on a series of reactors to obtain pure $H_2$ or reformate with the desired composition (mainly low CO concentration for application in some fuel cells) or a physical one (e.g. Pressure Swing Adsorption). Examples of membrane reactors are also available, allowing direct $H_2$ enrichment and purification [25-27].

## 3 - RESULTS AND DISCUSSION

### *3.1 – Effect of pressure, temperature and feed composition on the equilibrium composition*

The equilibrium composition has been at first calculated in the operating range of our interest. The reformer has been simulated (see part 2) at 750°C, 1.5-8.5 bar (1.8 bar has been mainly used for homogeneity with the experimental system used) and variable $H_2O$/

$C_2H_5OH$ ratio (5-14 mol/mol). Values are expressed as molar fraction on a dry basis as a function of temperature, pressure and $H_2O/C_2H_5OH$ feeding ratio for a system composed of $C_2H_5OH$, $H_2O$, $H_2$, $CO_2$, CO, $CH_4$, $C_2H_4$, $CH_3CHO$ and $(CH_3)_2CO$. Pressure was varied between 1 and 8.5 bar and the water/ethanol ratio between 3 and 18 mol/mol.

The equilibrium conditions were determined by setting up a simulation in Aspen Plus© using a Gibbs reactor model, *i.e.* by minimisation of the Gibbs free energy. The Gibbs reactor allows the determination of the equilibrium composition of a reacting system by specifying the valid phases and the compounds present in the reacting system, without the need of specifying the possible reactions and most of all without the preliminary knowledge of equilibrium constants. The reacting mixture above described has been used and deviations from ideality were taken into account by selecting the Peng – Robinson thermodynamic package, which is well fitted for a gas phase mainly consisting of light gases. An alternative selection may be the SRK model, which however gave identical results.

Some representative diagrams are reported in Fig.1 and 2, showing the effect of pressure and water/ethanol feeding ratio, respectively, on the equilibrium composition. Ethanol was found absent from product distribution in every case in the temperature range considered and the same applies for ethylene, acetaldehyde and acetone (maximum molar fraction $10^{-11}$). It can be noticed that an increase of pressure brings about a decrease of $H_2$ yield, mainly due to lower methane conversion. The macroscopic effect of the water/ethanol feeding ratio is then evident in Fig. 2. An increase of such parameter sensibly improves $H_2$ content at equilibrium even at low temperature by promoting effectively both the SRM and, above all, the WGS reactions.

*3.2. – Critical evaluation of literature kinetic models*

Different kinetic models have been found in the literature to describe various reaction schemes among those reported in section 2. They have been critically evaluated to find out the best solutions to implement our reactor models.

Most publications adopt a "power-rate law" approach [3,10,11,28-34]. Among these, some [10,11,34] refer to special reaction conditions, with proper temperature allowing ethanol dehydrogenation to acetaldehyde, which then decomposes to $CH_4$ and CO in the same reactor or is subsequently reformed in a second unit.

After some testing for process simulation the power rate law models have been discarded. In some cases unrealistically low activation energy is reported, likely due to non negligible diffusional problems [4,35]. However, more in general, the reaction conditions reported for the collection of all these data were markedly different with respect to the desired process conditions and, being such models derived by data fitting only, caution is needed during extrapolation to significantly different operating range.

Alternatively, Eley-Rideal type kinetic models are reported elsewhere [3,29-31]. An unrealistically low (7560 J $mol^{-1}$) activation energy is calculated in [3], ascribed later by the same authors [30] to diffusional limitations. Unfortunately, in all these papers a single reaction corresponding to the present R1 is used, without taking into consideration important byproducts such as CO and $CH_4$. For the purposes of the present work more detailed models are needed.

A *Langmuir-Hinshelwood* approach is used by Akpan et al. [30], compared with an Eley-Rideal one, but also in this case CO and $CH_4$ are not taken into account, and so this model can be used to predict ethanol conversion, only.

A more detailed approach is suggested by Arteaga et al. [12] for a $Ni/Al_2O_3$ catalyst, based on five different reactions, corresponding to the present R3, R10, R11, R12, R15 and R16. However, only the estimated kinetic constants are given, without temperature dependence and other thermodynamic parameters useful to model our process.

A microchannel reactor is considered elsewhere [36], but it has not been considered here due to too different fluid-dynamic regimes.

The most detailed approach has been found in the following three models, which have been considered more in detail and adapted to our system [4,35,37].

*3.2.1 – Model 1 [35]*

The following reaction scheme for SRE on $Co/Al_2O_3$ catalyst has been proposed by Sahoo et al. [35]. It was partially revised here with respect to the original version:

$$2S^* + CH_3CH_2OH(g) \overset{k_{1,-1}}{\longleftrightarrow} CH_3CH_2O^* + H^* \quad \text{(R18)}$$

$$S^* + CH_3CH_2O^* \overset{k_{2,-2}}{\longleftrightarrow} CH_3CHO^* + H^* \quad \text{(R19)}$$

$$2S^* + H_2O(g) \overset{k_{3,-3}}{\longleftrightarrow} OH^* + H^* \quad \text{(R20)}$$

$$CH_3CHO^* + H^* \overset{k_{4,-4}}{\longleftrightarrow} CH_3^* + HCHO^* \quad \text{(R21)}$$

$$CH_3^* + OH^* \overset{k_{5,-5}}{\longleftrightarrow} CH_3OH^* + S^* \quad \text{(R22)}$$

$$S^* + CH_3OH^* \overset{k_{6,-6}}{\longleftrightarrow} CH_3O^* + H^* \quad \text{(R23)}$$

$$CH_3O^* + S^* \overset{k_{7,-7}}{\longleftrightarrow} HCHO^* + H^* \quad \text{(R24)}$$

$$HCHO^* + OH^* \overset{k_{8,-8}}{\longleftrightarrow} HCOOH^* + H^* \quad \text{(R25)}$$

$$2S^* + HCOOH^* \overset{k_{9,-9}}{\longleftrightarrow} CO_2^* + 2H^* \quad \text{(R26)}$$

$$CO_2^* \overset{k_{10,-10}}{\longleftrightarrow} CO_2(g) + S^* \quad \text{(R27)}$$

$$2H^* \overset{k_{11,-11}}{\longleftrightarrow} H_2(g) + 2S^* \quad \text{(R28)}$$

$$S^* + HCOOH^* \overset{k_{12,-12}}{\longleftrightarrow} HCOO^* + H^* \quad \text{(R29)}$$

$$S^* + HCOO^* \overset{k_{13,-13}}{\longleftrightarrow} CO^* + OH^* \quad \text{(R30)}$$

$$CO^* \overset{k_{14,-14}}{\longleftrightarrow} CO(g) + S^* \quad \text{(R31)}$$

$$S^* + HCOO^* \overset{k_{15,-15}}{\longleftrightarrow} CO_2^* + H^* \quad \text{(R32)}$$

$$S^* + CH_3CHO^* \overset{k_{16,-16}}{\longleftrightarrow} CH_4^* + CO^* \quad \text{(R33)}$$

$$CH_4^* \overset{k_{17,-17}}{\longleftrightarrow} CH_4(g) + S^* \quad \text{(R34)}$$

S* denotes a free active site, whereas species marked with asterisks represent adsorbed molecules. According to the authors, reactions R19, R30 and R33 have been considered rate determining steps (RDS) for the SRE, WGS and ethanol decomposition (ED) reactions, respectively.

We redefined the formalisation of some elementary steps with respect to the original formulation, in particular: a) original reaction 17, now fixed as eq. R23; b) an incorrect stoichiometry of the original reaction 20, now fixed as in R26; c) an incorrect balance of adsorption sites in the original reaction 23, now fixed as R29.

This also ends in the different definition of the relative equilibrium constants, which have been conventionally calculated according to the stoichiometry above reported.

The concentration of the intermediates can be calculated by considering all the other reactions in a pseudo-equilibrium condition and by writing the corresponding equilibrium constants, together with a balance of active sites concentration, so that:

$$r_{SRE} = \frac{k_r K_{CH_3CH_2O^*}\left[\frac{[p_{C_2H_5OH}]}{[p_{H_2}]^{0,5}} - \frac{1}{K_{SRE}}\frac{[p_{CO_2}]^2[p_{H_2}]^{5,5}}{[p_{H_2O}]^3}\right][C_T]^2}{\left[1 + K_{CO_2^*}[p_{CO_2}] + K_{CO^*}[p_{CO}] + K_{CH_4^*}[p_{CH_4}] + K_{HCOO^*}[p_{CO_2}][p_{H_2}]^{0,5} + K_{H^*}[p_{H_2}]^{0,5} + K_{CH_3CHO^*}\frac{[p_{CO_2}]^2[p_{H_2}]^5}{[p_{H_2O}]^3} + K_{CH_3CH_2O^*}\frac{[p_{C_2H_5OH}]}{[p_{H_2}]^{0,5}} + K_{OH^*}\frac{[p_{H_2O}]}{[p_{H_2}]^{0,5}}\right]^2}$$

$$r_{WGS} = \frac{k_w K_{HCOO^*}\left[[p_{CO_2}][p_{H_2}]^{0,5} - \frac{1}{K_{WGS}}\frac{[p_{H_2O}][p_{CO}]}{[p_{H_2}]^{0,5}}\right][C_T]^2}{\left[1 + K_{CO_2^*}[p_{CO_2}] + K_{CO^*}[p_{CO}] + K_{CH_4^*}[p_{CH_4}] + K_{HCOO^*}[p_{CO_2}][p_{H_2}]^{0,5} + K_{H^*}[p_{H_2}]^{0,5} + K_{CH_3CHO^*}\frac{[p_{CO_2}]^2[p_{H_2}]^5}{[p_{H_2O}]^3} + K_{CH_3CH_2O^*}\frac{[p_{C_2H_5OH}]}{[p_{H_2}]^{0,5}} + K_{OH^*}\frac{[p_{H_2O}]}{[p_{H_2}]^{0,5}}\right]^2}$$

$$r_{\mathrm{ED}} = \frac{k_{\mathrm{d}} \mathrm{K}_{\mathrm{CH_3CHO^*}} \left[ \frac{[\mathrm{p}_{\mathrm{CO_2}}]^2 [\mathrm{p}_{\mathrm{H_2}}]^5}{[\mathrm{p}_{\mathrm{H_2O}}]^3} - \frac{1}{\mathrm{K}_{\mathrm{ED}}} [\mathrm{p}_{\mathrm{CH_4}}][\mathrm{p}_{\mathrm{CO}}] \right] [\mathrm{C_T}]^2}{\left[ 1 + \mathrm{K}_{\mathrm{CO_2^*}} [\mathrm{p}_{\mathrm{CO_2}}] + \mathrm{K}_{\mathrm{CO^*}} [\mathrm{p}_{\mathrm{CO}}] + \mathrm{K}_{\mathrm{CH_4^*}} [\mathrm{p}_{\mathrm{CH_4}}] + \mathrm{K}_{\mathrm{HCOO^*}} [\mathrm{p}_{\mathrm{CO_2}}][\mathrm{p}_{\mathrm{H_2}}]^{0,5} + \mathrm{K}_{\mathrm{H^*}} [\mathrm{p}_{\mathrm{H_2}}]^{0,5} + \mathrm{K}_{\mathrm{CH_3CHO^*}} \frac{[\mathrm{p}_{\mathrm{CO_2}}]^2 [\mathrm{p}_{\mathrm{H_2}}]^5}{[\mathrm{p}_{\mathrm{H_2O}}]^3} + \mathrm{K}_{\mathrm{CH_3CH_2O^*}} \frac{[\mathrm{p}_{\mathrm{C_2H_5OH}}]}{[\mathrm{p}_{\mathrm{H_2}}]^{0,5}} + \mathrm{K}_{\mathrm{OH^*}} \frac{[\mathrm{p}_{\mathrm{H_2O}}]}{[\mathrm{p}_{\mathrm{H_2}}]^{0,5}} \right]^2}$$

$r$ represents the reaction rate, $C_T$ the total concentration of active sites, $K_i$ adsorption equilibrium constants, $k_i$ kinetic constants. However, the attempt to use the kinetic parameters reported in [35] resulted in unreliable values calculated for the reaction rate. Therefore, we preferred to use this model to calculate the kinetic parameters by regression of the kinetic data reported in literature [4] and relative to a more representative $Ni/Al_2O_3$ catalyst. The material balances referred to each species resulted in the following set of differential equations, where $w$ is the mass of catalyst:

$$\frac{d\mathrm{CH_3CH_2OH}}{d\mathrm{t}}/w = -r_{\mathrm{SRE}}$$

$$\frac{d\mathrm{H_2O}}{d\mathrm{t}}/w = -3r_{\mathrm{SRE}} + r_{\mathrm{WGS}} + 3r_{\mathrm{ED}}$$

$$\frac{d\mathrm{H_2}}{d\mathrm{t}}/w = 6r_{\mathrm{SRE}} - r_{\mathrm{WGS}} - 5r_{\mathrm{ED}}$$

$$\frac{d\mathrm{CO_2}}{d\mathrm{t}}/w = 2r_{\mathrm{SRE}} - r_{\mathrm{WGS}} - 2r_{\mathrm{ED}}$$

$$\frac{d\mathrm{CO}}{d\mathrm{t}}/w = r_{\mathrm{WGS}} + r_{\mathrm{ED}}$$

$$\frac{d\mathrm{CH_4}}{d\mathrm{t}}/w = r_{\mathrm{ED}}$$

We were not able to adopt the kinetic parameters directly derived from the authors (Table 3 at p. 147 [35], because the enthalpies of adsorption were not specified.

*3.2.2 – Model 2 [4]*

An alternative reaction pathway has been discussed in [4] for the SRE on a $Ni/Al_2O_3$ catalyst:

$$CH_3CH_2OH(g) + S^* \overset{k_{a,-a}}{\longleftrightarrow} CH_3CH_2OH^* \quad \text{(R35)}$$

$$H_2O(g) + S^* \overset{k_{b,-b}}{\longleftrightarrow} H_2O^* \quad \text{(R36)}$$

$$CH_3CH_2OH^* \overset{k_c}{\rightarrow} CO(g) + CH_4^* + H_2(g) \quad \text{(R37)}$$

$$CH_3CH_2OH^* + H_2O^* \overset{k_d}{\rightarrow} CO_2(g) + CH_4^* + 2H_2(g) + S^* \quad \text{(R38)}$$

$$CH_4^* \overset{k_{e,-e}}{\longleftrightarrow} CH_4(g) + S^* \quad \text{(R39)}$$

$$CH_4^* + H_2O^* \overset{k_{f,-f}}{\longleftrightarrow} CO(g) + 3H_2(g) + 2S^* \quad \text{(R40)}$$

$$CH_4^* + 2H_2O^* \overset{k_{g,-g}}{\longleftrightarrow} CO_2(g) + 4H_2(g) + 3S^* \quad \text{(R41)}$$

Where R37, R38, R40 and R41 have been considered as RDS. The following reaction rates have been calculated as described for Model 1:

$$r_1 = \frac{k_1 K_E [p_{C_2H_5OH}][C_T]}{\left[1 + K_E[p_{C_2H_5OH}] + K_W[p_{H_2O}] + K_M[p_{CH_4}]\right]}$$

$$r_2 = \frac{k_2 K_E K_W [p_{C_2H_5OH}][p_{H_2O}][C_T]^2}{\left[1 + K_E[p_{C_2H_5OH}] + K_W[p_{H_2O}] + K_M[p_{CH_4}]\right]^2}$$

$$r_3 = \frac{k_3 K_M K_W \left[[p_{CH_4}][p_{H_2O}] - \frac{1}{K_3^{(g)}}[p_{CO}][p_{H_2}]^3\right][C_T]^2}{\left[1 + K_E[p_{C_2H_5OH}] + K_W[p_{H_2O}] + K_M[p_{CH_4}]\right]^2}$$

$$r_4 = \frac{k_4 K_M {K_W}^2 \left[[p_{CH_4}][p_{H_2O}]^2 - \frac{1}{K_4^{(g)}}[p_{CO_2}][p_{H_2}]^4\right][C_T]^3}{\left[1 + K_E[p_{C_2H_5OH}] + K_W[p_{H_2O}] + K_M[p_{CH_4}]\right]^3}$$

The material balances for each species give rise to the following set of differential equations:

$$\frac{d\mathrm{CH_3CH_2OH}}{d\mathrm{t}}/w = -r_1 - r_2$$

$$\frac{d\mathrm{H_2O}}{d\mathrm{t}}/w = -r_2 - r_3 - 2r_4$$

$$\frac{d\mathrm{H_2}}{d\mathrm{t}}/w = r_1 + 2r_2 + 3r_3 + 4r_4$$

$$\frac{d\mathrm{CO_2}}{d\mathrm{t}}/w = r_2 + r_4$$

$$\frac{d\mathrm{CO}}{d\mathrm{t}}/w = r_1 + r_3$$

$$\frac{d\mathrm{CH_4}}{d\mathrm{t}}/w = r_1 + r_2 - r_3 - r_4$$

Despite the authors provide all the numerical values needed to implement the system of kinetic equations, we have chosen to calculate such parameters by regression from the kinetic data reported in the same paper, for homogeneity with the other models.

*3.2.3 – Model 3 [37].*

A different kinetic scheme has been considered for a Rh(1wt%)$MgAl_2O_4$/$Al_2O_3$ catalyst [37].

$$\mathrm{CH_3CH_2OH(g)} + \mathrm{S^*} \overset{k_{1,-1}}{\longleftrightarrow} \mathrm{CH_3CH_2OH^*} \quad \text{(R42)}$$

$$\mathrm{CH_3CH_2OH^*} + \mathrm{S^*} \overset{k_{2,-2}}{\longleftrightarrow} \mathrm{CH_3CH_2O^*} + \mathrm{H^*} \quad \text{(R43)}$$

$$\mathrm{CH_3CH_2O^*} + \mathrm{S^*} \overset{k_3}{\rightarrow} \mathrm{CH_3CHO^*} + \mathrm{H^*} \quad \text{(R44)}$$

$$\mathrm{CH_3CHO^*} + \mathrm{S^*} \overset{k_4}{\rightarrow} \mathrm{CH_3^*} + \mathrm{CHO^*} \quad \text{(R45)}$$

$$\mathrm{CHO^*} + \mathrm{S^*} \overset{k_5}{\rightarrow} \mathrm{CO^*} + \mathrm{H^*} \quad \text{(R46)}$$

$$\mathrm{CH_3^*} + \mathrm{H^*} \overset{k_{6,-6}}{\longleftrightarrow} \mathrm{CH_4^*} + \mathrm{S^*} \quad \text{(R47)}$$

$$CHO^* + OH^* \xrightarrow{k_7} CO_2^* + H_2(g) + S^* \quad \text{(R48)}$$

$$H_2O(g) + 2S^* \overset{k_{8,-8}}{\longleftrightarrow} OH^* + H^* \quad \text{(R49)}$$

$$CH_4^* \overset{k_{9,-9}}{\longleftrightarrow} CH_4(g) + S^* \quad \text{(R50)}$$

$$CO^* \overset{k_{10,-10}}{\longleftrightarrow} CO(g) + S^* \quad \text{(R51)}$$

$$CO_2^* \overset{k_{11,-11}}{\longleftrightarrow} CO_2(g) + S^* \quad \text{(R52)}$$

$$2H^* \overset{k_{12,-12}}{\longleftrightarrow} H_2(g) + 2S^* \quad \text{(R53)}$$

$$CH_3^* + OH^* \overset{k_{13,-13}}{\longleftrightarrow} CO^* + 2H_2(g) + S^* \quad \text{(R54)}$$

$$CO^* + OH^* \overset{k_{14,-14}}{\longleftrightarrow} CO_2^* + H^* \quad \text{(R55)}$$

Where reactions R46, R48, R54, R55 have been considered as RDS for ED, SRE, SRM and WGS, respectively. Following the same approach used for Models 1 and 2 we obtained:

$$r_{ED} = \frac{k_5 N \frac{[p_{C_2H_5OH}]}{[p_{CH_4}][p_{H_2}]^{0,5}} [C_T]^2}{\left[1 + A[p_{C_2H_5OH}] + C\frac{[p_{CH_4}]}{[p_{H_2}]^{0,5}} + F\frac{[p_{H_2O}]}{[p_{H_2}]^{0,5}} + G[p_{CH_4}] + H[p_{CO}] + I[p_{CO_2}] + J[p_{H_2}]^{0,5} + L\frac{[p_{C_2H_5OH}]}{[p_{H_2}]^{0,5}} + M\frac{[p_{C_2H_5OH}]}{[p_{H_2}]} + N\frac{[p_{C_2H_5OH}]}{[p_{CH_4}][p_{H_2}]^{0,5}}\right]^2}$$

$$r_{SRE} = \frac{k_7 NF \frac{[p_{C_2H_5OH}][p_{H_2O}]}{[p_{CH_4}][p_{H_2}]} [C_T]^2}{\left[1 + A[p_{C_2H_5OH}] + C\frac{[p_{CH_4}]}{[p_{H_2}]^{0,5}} + F\frac{[p_{H_2O}]}{[p_{H_2}]^{0,5}} + G[p_{CH_4}] + H[p_{CO}] + I[p_{CO_2}] + J[p_{H_2}]^{0,5} + L\frac{[p_{C_2H_5OH}]}{[p_{H_2}]^{0,5}} + M\frac{[p_{C_2H_5OH}]}{[p_{H_2}]} + N\frac{[p_{C_2H_5OH}]}{[p_{CH_4}][p_{H_2}]^{0,5}}\right]^2}$$

$$r_{SRM} = \frac{k_{13} CF\left[\frac{[p_{CH_4}][p_{H_2O}]}{[p_{H_2}]} - \frac{1}{K_{SRM}}[p_{CO}][p_{H_2}]^2\right][C_T]^2}{\left[1 + A[p_{C_2H_5OH}] + C\frac{[p_{CH_4}]}{[p_{H_2}]^{0,5}} + F\frac{[p_{H_2O}]}{[p_{H_2}]^{0,5}} + G[p_{CH_4}] + H[p_{CO}] + I[p_{CO_2}] + J[p_{H_2}]^{0,5} + L\frac{[p_{C_2H_5OH}]}{[p_{H_2}]^{0,5}} + M\frac{[p_{C_2H_5OH}]}{[p_{H_2}]} + N\frac{[p_{C_2H_5OH}]}{[p_{CH_4}][p_{H_2}]^{0,5}}\right]^2}$$

$$r_{WGS} = \frac{k_{14} HF\left[\frac{[p_{CO}][p_{H_2O}]}{[p_{H_2}]^{0,5}} - \frac{1}{K_{WGS}}[p_{CO_2}][p_{H_2}]^{0,5}\right][C_T]^2}{\left[1 + A[p_{C_2H_5OH}] + C\frac{[p_{CH_4}]}{[p_{H_2}]^{0,5}} + F\frac{[p_{H_2O}]}{[p_{H_2}]^{0,5}} + G[p_{CH_4}] + H[p_{CO}] + I[p_{CO_2}] + J[p_{H_2}]^{0,5} + L\frac{[p_{C_2H_5OH}]}{[p_{H_2}]^{0,5}} + M\frac{[p_{C_2H_5OH}]}{[p_{H_2}]} + N\frac{[p_{C_2H_5OH}]}{[p_{CH_4}][p_{H_2}]^{0,5}}\right]^2}$$

The material balances for each species are the following:

$$\frac{d\mathrm{CH_3CH_2OH}}{d\mathrm{t}}/w = -r_{\mathrm{ED}} - r_{\mathrm{SRE}}$$

$$\frac{d\mathrm{H_2O}}{d\mathrm{t}}/w = -r_{\mathrm{SRE}} - r_{\mathrm{SRM}} - r_{\mathrm{WGS}}$$

$$\frac{d\mathrm{H_2}}{d\mathrm{t}}/w = r_{\mathrm{ED}} + 2r_{\mathrm{SRE}} + 3r_{\mathrm{SRM}} + r_{\mathrm{WGS}}$$

$$\frac{d\mathrm{CO_2}}{d\mathrm{t}}/w = r_{\mathrm{SRE}} + r_{\mathrm{WGS}}$$

$$\frac{d\mathrm{CO}}{d\mathrm{t}}/w = r_{\mathrm{ED}} + r_{\mathrm{SRM}} - r_{\mathrm{WGS}}$$

$$\frac{d\mathrm{CH_4}}{d\mathrm{t}}/w = r_{\mathrm{ED}} + r_{\mathrm{SRE}} - r_{\mathrm{SRM}}$$

The expressions for A-N are reported in the original paper [37]. The present kinetic equations have been revised for some errors. The authors in this case do not provide most of the numerical values needed to implement the system of kinetic equations. Then we calculated the parameters by regression from the experimental data given in [4] as for the previous models.

It should be remarked that the authors report in their Table 1 [37] the definitions of the parameters A-N (same nomenclature as ours), which describe the adsorption constants of the different species as combination of the equilibrium constants of previously defined elementary steps. Some incongruences appear, such as the definition of the constant C, relative to the desorption of the $CH_3$* species is likely a copy-paste from the previous line; the desorption steps of $H_2$, CO, $CO_2$ and $CH_4$ appear formalised as adsorption.

They also report alternative formulations for the constants L, M and N (respectively: E, D and B). However, it appears that these should refer to a different model, because the constant $K_5$ is included, which refers to a rate determining step in Model 3. Thus, it is incorrect to define it at equilibrium and to use it to calculate the concentration of any

intermediate. The authors should also have inverted the terms between parentheses at the numerator of $r_{WGS}$ and $r_{SRM}$, because in the original paper $r_{WGS}$ depends of $y_{CH4}$, while $r_{SRM}$ on $y_{CO}$.

At last, it should be noticed that no model is currently available to predict the coking rate of ethanol steam reforming catalysts. Therefore, the operating conditions should be selected in a conservative way, *i.e*. overstoichiometric water ethanol feeding ratio and high temperature (usually T>600°C).

*3.3 – Estimation of kinetic parameters*

The implementation of a kinetic model in Aspen Plus© to simulate the steam reforming reactor, which will be object of the second part of this work, requires the calculation of the kinetic and thermodynamic (*e.g*. adsorption) constants appearing in the kinetic equation under variable reaction conditions. None of the selected publications fully described the set of parameters needed (pre-exponential factors, activation energies, adsorption enthalpies, etc.). Therefore, we searched for a sufficiently broad and representative data set [4] and we newly regressed those data applying the three selected models, to get the required kinetic parameters to describe the system.

The experimental data extrapolated from [4] have been summarised in Table 1. To obtain the experimental profiles of the other species outflowing from the reactor and required by the model, but not reported in the paper, *e.g.* $CH_4$ and $H_2O$, we applied C, H and O balances. C balance is considered reliable since the authors claim less than 5% C loss. Furthermore, no ethylene, nor acetaldehyde are reported by the authors among the observed products. The calculated values for $CH_4$ and $H_2O$ outflowing from the reactor are also reported in Table 1.

The equilibrium constants for some of the reactions for the three models have been calculated as a function of temperature (125-750°C) using the following equations:

$$\Delta_r G^T = \Delta_r H^T - T\Delta_r S^T$$

$$\Delta_r H^T = \sum_i \left[\nu_i \Delta_f H_i^T\right]$$

$$\Delta_r S^T = \sum_i \left[\nu_i S_i^T\right]$$

$$\Delta_f H_i^T = \Delta_f H_i^0 + \int c_p dT$$

$$S_i^T = S_i^0 + \int (c_p/T) dT$$

$$\ln(K_{eq}) = -\frac{\Delta_r G^T}{RT}$$

$$K_{eq} = K_0 e^{\frac{-\Delta_r H}{RT}}$$

The calculated values of $K_0$ and $-\Delta_r H$ are reported in Table 2.

Both Athena Visual Studio© and Matlab© scripts have been developed to integrate the set of differential equations describing the mass balances for each species entering/forming in the reactor and to apply a least square algorithm to the calculated molar flows of each of them outflowing from the reactor. The calculated values have been compared with the experimental ones reported in Table 1 to estimate the kinetic parameters for each model. The inlet values of the molar flow rates for ethanol and water have been set as reported in [4]. Since the fugacities of some components appear as denominator of some quotient, their initial values have been set as $10^{-8}$ mol/s, in particular $H_2$ and $CH_4$ for Model 3 and $H_2$ for Model 1.

Different optimization algorithms have been tested. A derivative-free approach based on the simplex method was preferred. Other algorithms available in Matlab©, specifically conceived for data-fitting purposes, resulted extremely slow due to the huge number of numerically calculated derivatives needed for each iteration [38,39]. A further simplification of the

minimum search was in case achieved by using the kinetic and adsorption constants at each temperature as parameters to be estimated, instead of the Arrhenius and Van't Hoff parameters of each of them. The latter have been calculated separately by regression of the optimized constants *vs.* 1/T.

$$\ln(k_{\mathrm{i}}) = \ln(k_{0\mathrm{i}}) - (\mathrm{Ea_i}/\mathrm{R})\frac{1}{\mathrm{T}}$$

$$\ln(\mathrm{K_j}) = \ln(\mathrm{K_{0j}}) - (\Delta\mathrm{H_j}/\mathrm{R})\frac{1}{\mathrm{T}}$$

The total sum of squares (TSS) has been calculated as follows for a given temperature:

$$\mathrm{TSS_T} = \sum_j \sum_{\mathrm{i}} \left[(\hat{\mathrm{n}}_{\mathrm{i}} - \mathrm{n}_{\mathrm{i}})_{\mathrm{j}}^2\right]$$

where the calculated and experimental values were indicated with and without the superscript, respectively, *i* refers to each space velocity (catalyst mass) and *j* represents the different chemical species. Additionally, the determination coefficients $R^2$ have been defined as:

$$\mathrm{R^2_{T,j}} = 1 - \frac{\sum_{\mathrm{i}}(\hat{\mathrm{n}}_{\mathrm{i}} - \mathrm{n}_{\mathrm{i}})_{\mathrm{j}}^2}{\sum_{\mathrm{i}}(\bar{\mathrm{n}}_{\mathrm{i}} - \mathrm{n}_{\mathrm{i}})_{\mathrm{j}}^2}$$

$\bar{n}_i$ being the mean of the experimental values for the species *j* at temperature T.

Different scripts have been prepared for the different kinetic models. The optimization routine made use of the Optimization Toolbox© and included the call to the model, integrated through the ODE15s function and the calculation of the sum of the residual square above reported.

The results are reported in Tables 3-5. Missing parameters in those Tables are due to their nil values obtained during the optimization.

The comparison between the calculated and experimental values of molar flows across the reactor are reported in Fig. 3 and 4 for the three models. Model 1 does not allow to predict a reliable profile for $CH_4$. Indeed, notice that the y-axis for $CH_4$ in Fig. 3 has an order of magnitude $10^{-10}$, to be compared with the experimental values in the order $10^{-6}$ (Fig. 4). A

more reliable profile is predicted by Models 2 and 3. Unfortunately, no direct experimental data are available for $CH_4$, so its molar flow is characterized by high uncertainty. Model 3 is characterized by smaller TSS and higher $R^2$ values than Model 2, and the former better represents CO evolution than the latter. The parity plot for Model 3 is reported in Fig. 5.

A comparison of the kinetic parameters here determined with literature values has been attempted. A trustful comparison is inhibited by the publication of incomplete data and by the difference of models' formulations. The most complete inventory of data is reported by Graschinsky et al. [37], who compared the activation energies of different models found in the literature. Unfortunately, only such parameter is comparatively reported, and this may lead to misleading conclusions. Indeed, the two Arrhenius parameters may be correlated, so that an apparently higher activation energy, coupled with a much higher preexponential factor may lead in many cases to successful results. By comparing the activation energies of Table 5 with the activation energies reported in [37], one may notice that the value of activation energy characterized the ED reaction of this Ni-based sample, was much higher than what reported for the original Rh-based catalyst. In contrast, the activation energy for the SRE reaction was the lowest, implying that ethanol decomposition (and the subsequent reforming of methane are the limiting steps of the reaction. WGS parameters are lower than most of the data reported and in line with those of Sahoo et al. [35,37]. However, the real kinetically limited process is methane steam reforming. Indeed the ED reaction has the highest activation energy among those here reported, but it is accompanied by the highest preexponential factor. This implies that in the investigated temperature range, the overall value of the kinetic constant of the ED reaction is *ca*. 3000 times higher than that of SRM.

The kinetic and thermodynamic parameters presently determined according to Model 3 were found suitable to describe the behavior of a steam reformer in an accurate way. Furthermore, the model was applied to a different data set with respect to that for which it was originally derived, demonstrating able to describe the behavior of widely different

catalytic systems (Rh and Ni-based ones). Therefore, Model 3 has been used to simulate the steam reforming unit described in the second part of this work with the parameters here estimated.

## 4 – CONCLUSIONS

In order to simulate and optimise the performance of a steam reforming unit, coupled with a fuel cell, a reliable kinetic model is needed, together with sound kinetic and thermodynamic parameters. A revision of the pertinent literature models is here proposed. Due to some imprecisions and missing data, some models have been here revised and applied to available kinetic data. Model 3 was found the most representative and thermodynamically consistent among those here evaluated. It also proved sufficiently versatile to be successfully applied to different data sets, *i.e.* it well represented the Rh-based catalyst for which it was originally derived and the presently selected Ni-based catalyst (of course giving rise to a different set of kinetic parameters). The kinetic and thermodynamic data were estimated by developing proper methods and scripts for the integration of the set of differential equations describing mass balances for each compound and by applying a least square algorithm for the optimization of parameters values. Model 3 with its estimated parameters has been used to simulate a $H_2$ production unit to feed a 5 $kW_{electric}$ + 5 $kW_{thermal}$ unit, as described in part 2.

## REFERENCES


1. P. Ramìrez de la Piscina, N. Homs, Chem. Soc. Rev., 2008, 37, 2459-2467.
2. http://betarenewables.neencloud.it/proesa/what-is

3. A. Akande, A. Aboudheir, R. Idem, A. Dalai, Int. J. Hydrogen Energy, 31 (2006) 1707-1715.
4. V. Mas, M.L. Bergamini, G. Baronetti, N. Amadeo, M. Laborde, Top. Catal. 51 (2008) 39-48.
5. L. Hernández, V. Kafarov, J. Appl. Sci., 7 (2007) 2015-2019.
6. I. Rossetti, J. Lasso, M. Compagnoni, G. De Guido, L. Pellegrini, Chem. Eng. Trans., in press.
7. W. Jamsak, P.L. Douglas, E. Croiset, R. Suwanwarangkul, N. Laosiripojana, S. Charojrochkul, S. Assabumrungrat, J. Power Sources, 187 (2009) 190-203.
8. I. Rossetti, C. Biffi, G.F. Tantardini, M. Raimondi, E. Vitto, D. Alberti, Int. J. Hydrogen Energy, 37(12) (2012) 8499-8504.
9. A.N. Fatsikostas, X.E. Verykios, J. Catal., 225 (2004) 439–452.
10. D.A. Morgenstern, J.P. Fornango, Energy & Fuels, 19 (2005) 1708-1716.
11. V.M. García, E. López, M. Serra, J. Llorca, J. Power Sources, 192 (2009) 208-215.
12. L.E. Arteaga, L.M. Peralta, Vi. Kafarov, Y. Casas, E. Gonzales, Chem. Eng. J., 136 (2008) 256-266.
13. P. Djinovic, C. Galletti, S. Specchia, V. Specchia, Catal. Today, 164 (2011) 282-287.
14. M. Benito, R. Padilla, A. Serrano-Lotina, L. Rodríguez, J.J. Brey, L. Daza, J. Power Sources, 192 (2009) 158–164.
15. P.D. Vaidya, A.E. Rodrigues, Chem. Eng. J., 117 (2006) 39-49.
16. V. Nichele, M. Signoretto, F. Pinna, F. Menegazzo, I. Rossetti, G. Cruciani, G. Cerrato, A. Di Michele, Appl. Catal. B: Environ., 150-151 (2014) 12-20.
17. F. Díaz Alvarado, F. Gracia, Chem. Eng. J., 165 (2010) 649-657.
18. I. Rossetti, J. Lasso, E. Finocchio, G. Ramis, V. Nichele, M. Signoretto, A. Di Michele, Appl. Catal. B: Environmental, 150-151 (2014) 257-267.

19. I. Rossetti, C. Biffi, C. Bianchi, V. Nichele, M. Signoretto, F. Menegazzo, E. Finocchio, G. Ramis, A. Di Michele, Appl. Catal. B: Environmental, 117-118 (2012) 384-396.
20. I. Rossetti, J. Lasso, E. Finocchio, G. Ramis, V. Nichele, M. Signoretto, A. Di Michele, Appl. Catal. A: General, 477 (2014) 42–53.
21. V. Nichele, M. Signoretto, F. Menegazzo, I. Rossetti, G. Cruciani, Int. J. Hydrogen Energy, 39 (2014) 4252-4258.
22. I. Rossetti, A. Gallo, V. Dal Santo, C.L. Bianchi, V. Nichele, M. Signoretto, E. Finocchio, G. Ramis, G. Garbarino, A. Di Michele, ChemCatChem, 5 (2013) 294-306.
23. I. Dancini-Pontes, M. De Souza, F.A. Silva, M.H.N. Olsen Scaliante, C.G. Alonso, G.S. Bianchi, A. Medina Neto, G. Mirada Pereira, N.R.C. Fernandes-Machado, Chem. Eng. J., 273 (2015) 66.
24. A. Kumar, A. Cross, K. Manukyan, R.R. Bhosale, L.J.P. van den Broeke, J.T. Miller, A.S. Mukasyan, E.E. Wolf, Chem. Eng. J., 278 (2015) 46.
25. S. Tosti, C. Cavezza, M. Fabbricino, L. Pontoni, V. Palma, C. Ruocco, Chem. Eng. J., 275 (2015) 366.
26. Y.S. Cheng, M.A. Pena, K.L. Yeung, J. Taiwan Institute of Chem Eng., 40 (2009) 281.
27. K.L. Yeung, R. Aravind, J. Szegner, A. Varma, Stud. Surf. Sci. Catal., 101 (1996) 1349.
28. A. Therdthianwong, T. Sakulkoakiet, S. Therdthianwong, Science Asia, 27 (2001) 193-198.
29. P.D. Vaidya, A.E. Rodrigues, Ind. Eng. Chem. Res., 45 (2006) 6614-6618.
30. E. Akpan, A. Akande, A. Aboudheir, H. Ibrahim, R. Idem, Chem. Eng. Sci., 62 (2007) 3112-3126.
31. P.V. Mathure, S. Ganguly, A.V. Patwardhan, R.K. Saha, Ind. Eng. Chem. Res., 46 (2007) 8471-8479.
32. V. Mas, G. Baronetti, N. Amadeo, M. Laborde, Chem. Eng. J., 138 (2008) 602–607.

33. P. Ciambelli, V. Palma, A. Ruggiero, Appl. Catal. B: Environmental, 96 (2010) 190-19.
34. V.M. García, M. Serra, J. Llorca, J. Power Sources, 196 (2011) 4411-4417.
35. D.R. Sahoo, S. Vajpai, S. Patel, K.K. Pant, Chem. Eng. J., 125 (2007) 139-147.
36. O. Görke, P. Pfeifer, K. Schubert, Appl. Catal. A: General, 360 (2009) 232-241.
37. C. Graschinsky, M. Laborde, N. Amadeo, A.L. Valant, N. Bion, F. Epron, D. Duprez, Ind. Eng. Chem. Res., 49 (2010) 12383-12389.
38. J.C. Lagarias, J.A. Reeds, M.H. Wright, P.E. Wright, SIAM Journal of Optimization, 9 (1998) 112-147.
39. T.F. Coleman, Y. Li, Mathematical Programming, 67 (1994) 189-224.

**Table 1:** Ethanol conversion and yield to selected products, calculated as mol per mol of ethanol. Original data reported in [10]. The inlet molar flows are 1.4647 mmol $min^{-1}$ and 0.26040 mmol $min^{-1}$ for ethanol and water, respectively. The yield of $CH_4$ and outflowing $H_2O$ have been calculated by C, H and O balances.

| Space-time | **Experimental** | | | | **Calculated** | |
|---|---|---|---|---|---|---|
| $g_{cat}$ min $mol^{-1}$ | Conv.% | $H_2$ yield | $CO_2$ yield | CO yield | $CH_4$ yield | $H_2O/C_2H_5OH_{in}$ |
| | **823 K** | | | | | |
| 0.000 | 0.000 | 0.000 | 0.000 | 0.000 | 0.000 | 5.625 |
| 0.252 | 20.400 | 1.100 | 0.330 | 0.075 | 0.007 | 5.107 |
| 0.379 | 27.000 | 1.410 | 0.400 | 0.122 | 0.020 | 4.979 |
| 0.429 | 28.000 | 1.440 | 0.350 | 0.083 | 0.091 | 5.001 |
| 0.503 | 41.700 | 2.250 | 0.650 | 0.188 | 0.004 | 4.582 |
| 0.647 | 39.500 | 2.120 | - | 0.204 | 0.012 | 4.667 |
| 0.660 | 49.200 | 2.620 | - | 0.252 | 0.020 | 4.441 |
| | **873 K** | | | | | |
| 0.000 | 0.000 | 0.000 | 0.000 | 0.000 | 0.000 | 5.625 |
| 0.123 | 18.000 | 0.750 | 0.225 | 0.053 | 0.077 | 5.284 |
| 0.175 | 39.200 | 1.090 | 0.295 | 0.118 | 0.336 | 5.192 |
| 0.276 | 50.400 | 3.240 | - | - | - | - |
| 0.293 | 45.900 | 2.240 | 0,595 | 0.199 | 0.105 | 4.633 |
| 0.368 | 63.600 | 3.390 | 0.870 | 0.337 | 0.022 | 4.099 |
| 0.394 | 60.000 | 2.710 | 0.735 | 0.272 | 0.155 | 4.406 |
| 0.441 | 68.000 | 3.240 | 0.810 | 0.363 | 0.119 | 4.187 |
| 0.510 | 76.000 | 3.890 | 1.030 | 0.418 | 0.063 | 3.889 |
| 0.573 | 80.900 | 3.730 | - | 0.392 | 0.183 | 3.956 |
| | **898 K** | | | | | |
| 0.000 | 0.000 | 0.000 | 0.000 | 0.000 | 0.000 | 5.625 |
| 0.111 | 35.900 | 1.920 | 0.515 | 0.193 | 0.010 | 4.761 |
| 0.179 | 54.100 | 2.600 | 0.680 | 0.292 | 0.101 | 4.484 |
| 0.273 | 71.800 | 3.610 | 0.930 | 0.420 | 0.079 | 4.040 |
| 0.322 | 77.200 | 3.820 | 0.985 | 0.455 | 0.098 | 3.952 |
| 0.420 | 84.700 | 4.460 | 1.130 | 0.557 | 0.011 | 3.668 |
| 0.558 | 97.000 | 4.770 | 1.165 | 0.651 | 0.114 | 3.581 |
| | **923 K** | | | | | |
| 0.000 | 0.000 | 0.000 | 0.000 | 0.000 | 0.000 | 5.625 |
| 0.099 | 51.600 | 2.640 | 0.655 | 0.353 | 0.025 | 4.480 |
| 0.135 | 62.600 | 3.290 | 0.780 | 0.477 | 0.000 | 4.217 |
| 0.196 | 80.900 | 4.020 | 0.970 | 0.577 | 0.068 | 3.908 |
| 0.239 | 87.500 | 4.280 | 1.050 | 0.606 | 0.093 | 3.790 |
| 0.270 | 94.200 | 4.810 | 1.105 | 0.748 | 0.028 | 3.599 |
| 0.368 | 98.600 | 5.070 | 1.195 | 0.774 | 0.009 | 3.468 |

**Table 2:** Temperature dependence of the equilibrium constants of some reactions.

| **Model 1** | | | | | |
|---|---|---|---|---|---|
| $K_{SRE}$ | | $K_{WGS}$ | | $K_{ED}$ | |
| $\ln(K_0)$ | $-\Delta_rH/R$ | $\ln(K_0)$ | $-\Delta_rH/R$ | $\ln(K_0)$ | $-\Delta_rH/R$ |
| 50.1 | -23458.9 | -4.3 | 4626.3 | -20.8 | 17076.2 |
| **Model 2** | | | | | |
| $K_3^{(g)}$ | | $K_4^{(g)}$ | | | |
| $\ln(K_0)$ | $-\Delta_rH/R$ | $\ln(K_0)$ | $-\Delta_rH/R$ | | |
| 29.3 | -26211.7 | 25.0 | -21585.3 | | |
| **Model 3** | | | | | |
| $K_{SRM}$ | | $K_{WGS}$ | | | |
| $\ln(K_0)$ | $-\Delta_rH/R$ | $\ln(K_0)$ | $-\Delta_rH/R$ | | |
| 29.3 | -26211.7 | -4.3 | 4626.3 | | |

**Table 3:** Results of Model 1 implementation and estimated kinetic and adsorption parameters. TSS = Total Sum of Squares.

| Model 1 | | | | |
|---|---|---|---|---|
| | 823 K | 873 K | 898 K | 923 K |
| TSS [$mol^2\ s^{-2}$] | 1.237E-11 | 8.254E-11 | 2.171E-11 | 1.004E-11 |
| $R^2_{CH3CH2OH}$ | 0.7165 | 0.9330 | 0.9561 | 0.9374 |
| $R^2_{H2O}$ | 0.7884 | 0.6992 | 0.8889 | 0.9434 |
| $R^2_{H2}$ | 0.8121 | 0.7411 | 0.9021 | 0.9376 |
| $R^2_{CO2}$ | 0.6872 | 0.6590 | 0.8944 | 0.9263 |
| $R^2_{CO}$ | 0.0137 | 0.8783 | 0.8468 | 0.7917 |

| Model1 | | | | | | | | |
|---|---|---|---|---|---|---|---|---|
| | mol $s^{-1}$ $g^{-1}$ | | | J $mol^{-1}$ | | | | J $mol^{-1}$ |
| $k_{0r}$ | 4.332E+00 | | $Ea_r$ | 38150 | $K_{0CO2*}$ | 1.115E-03 | $\Delta H_{CO2*}$ | -10543 |
| $k_{0w}$ | 2.393E+04 | | $Ea_w$ | 64247 | $K_{0CO*}$ | 1.417E-02 | $\Delta H_{CO*}$ | -47295 |
| $k_{0d}$ | 1.048E+07 | | $Ea_d$ | 122649 | $K_{0HCOO*}$ | 7.003E-07 | $\Delta H_{HCOO*}$ | -160270 |
| | | | | | $K_{0CH3CHO*}$ | 1.533E-02 | $\Delta H_{CH3CHO*}$ | -35371 |
| | | | | | $K_{0CH3CH2O*}$ | 9.707E-04 | $\Delta H_{CH3CH2O*}$ | -87143 |
| | | | | | $K_{0OH*}$ | 3.868E-02 | $\Delta H_{OH*}$ | -38250 |

**Table 4:** Results of Model 2 implementation and estimated kinetic and adsorption parameters. TSS = Total Sum of Squares.

| Model 2 | | | | |
|---|---|---|---|---|
| | 823 K | 873 K | 898 K | 923 K |
| TSS [$mol^2\ s^{-2}$] | 4.771E-11 | 4.726E-11 | 1.013E-11 | 1.562E-11 |
| $R^2_{CH3CH2OH}$ | 0.5776 | 0.8059 | 0.9456 | 0.9833 |
| $R^2_{H2O}$ | 0.0353 | 0.7943 | 0.9407 | 0.9264 |
| $R^2_{H2}$ | 0.1492 | 0.7216 | 0.9548 | 0.9044 |
| $R^2_{CO2}$ | 0.1272 | 0.6472 | 0.9579 | 0.9754 |
| $R^2_{CO}$ | 0.7217 | 0.6011 | 0.8811 | 0.6858 |

| Model 2 | | | | | | | | |
|---|---|---|---|---|---|---|---|---|
| | $mol\ s^{-1}\ g^{-1}$ | | | $J\ mol^{-1}$ | | | | $J\ mol^{-1}$ |
| $k_{01}$ | 2.991E+14 | | $Ea_1$ | 304529 | $K_{0E}$ | 3.781E-02 | $\Delta H_E$ | -60978 |
| $k_{02}$ | 8.835E+10 | | $Ea_2$ | 210596 | $K_{0W}$ | 4.792E-12 | $\Delta H_W$ | -187349 |
| $k_{03}$ | 4.596E+10 | | $Ea_3$ | 166619 | $K_{0M}$ | 6.526E-08 | $\Delta H_M$ | -126795 |
| $k_{04}$ | 4.459E+28 | | $Ea_4$ | 428652 | | | | |

**Table 5:** Results of Model 3 implementation and estimated kinetic and adsorption parameters. TSS = Total Sum of Squares.

| Model 3 | | | | |
|---|---|---|---|---|
| | 823 K | 873 K | 898 K | 923 K |
| TSS [$mol^2\ s^{-2}$] | 1.217E-11 | 3.420E-11 | 5.031E-12 | 4.479E-12 |
| $R^2_{CH3CH2OH}$ | 0.5019 | 0.8892 | 0.9920 | 0.9994 |
| $R^2_{H2O}$ | 0.6997 | 0.8624 | 0.9606 | 0.9975 |
| $R^2_{H2}$ | 0.7398 | 0.8192 | 0.9721 | 0.9977 |
| $R^2_{CO2}$ | 0.6868 | 0.8188 | 0.9612 | 0.9978 |
| $R^2_{CO}$ | 0.0539 | 0.7852 | 0.9964 | 0.9941 |

| Model 3 | | | | | | | | |
|---|---|---|---|---|---|---|---|---|
| | $mol\ s^{-1}\ g^{-1}$ | | | $J\ mol^{-1}$ | | | | $J\ mol^{-1}$ |
| $k_{05}$ | 1.544E+20 | | $Ea_5$ | 302980 | $C_0$ | 2.926E-02 | $\Delta H_C$ | -55199 |
| $k_{07}$ | 1.920E+05 | | $Ea_7$ | 41605 | $F_0$ | 2.412E-04 | $\Delta H_F$ | -76661 |
| $k_{013}$ | 7.756E+09 | | $Ea_{13}$ | 187783 | $G_0$ | 9.940E+01 | $\Delta H_G$ | -13965 |
| $k_{014}$ | 5.044E+05 | | $Ea_{14}$ | 56252 | $H_0$ | 2.322E+00 | $\Delta H_H$ | 27945 |
| | | | | | $I_0$ | 4.907E-02 | $\Delta H_I$ | -67738 |
| | | | | | $M_0$ | 1.369E-01 | $\Delta H_M$ | -32808 |
| | | | | | $N_0$ | 1.660E-05 | $\Delta H_N$ | 16489 |

## FIGURES

**Fig. 1:** Equilibrium composition for SRE on a dry basis as a function of temperature at variable pressure.

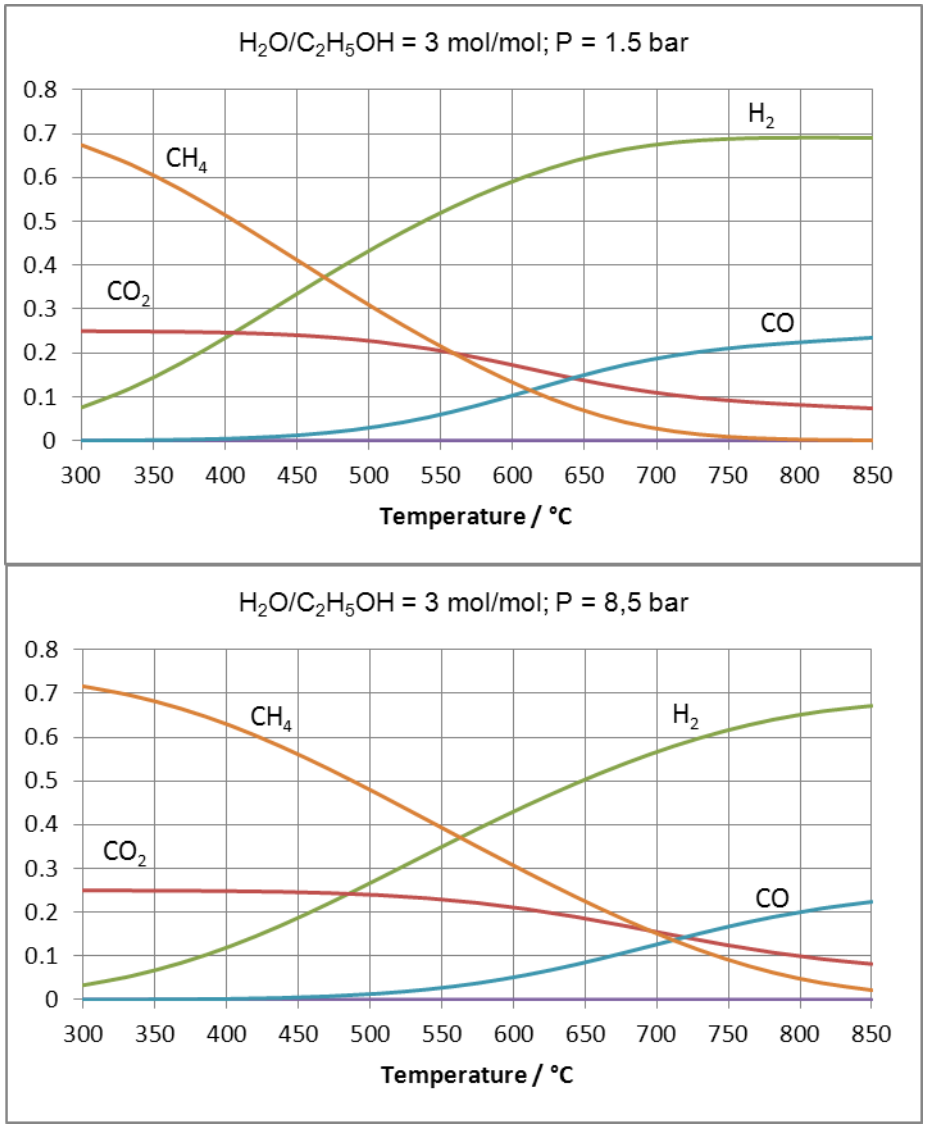

**Fig. 2:** Equilibrium composition for SRE on a dry basis as a function of temperature at variable water/ethanol feeding ratio.

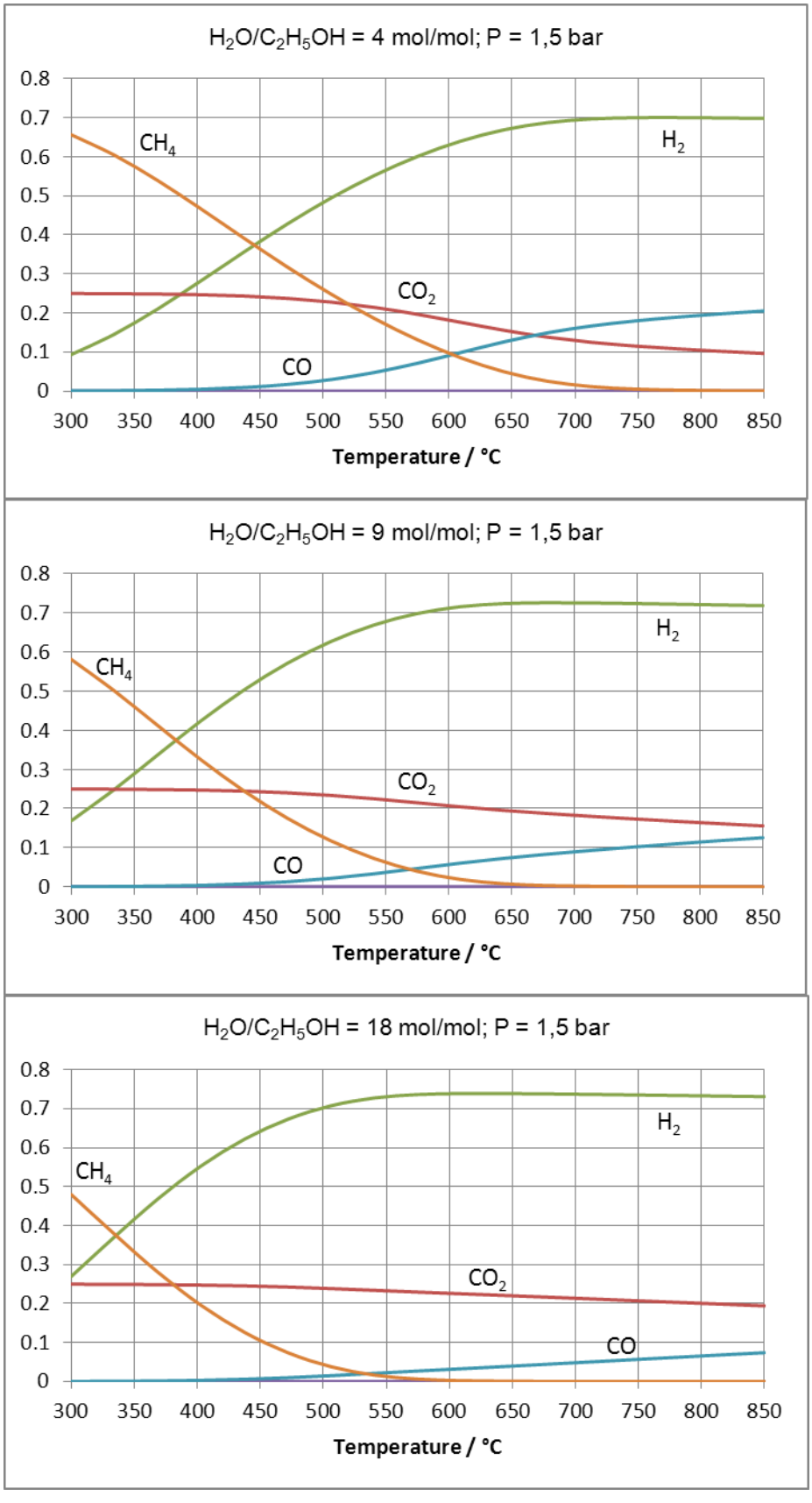

**Fig. 3:** Calculated (continuous line) *vs*. experimental values reported in Table 1 according to Model 1 at different temperature.

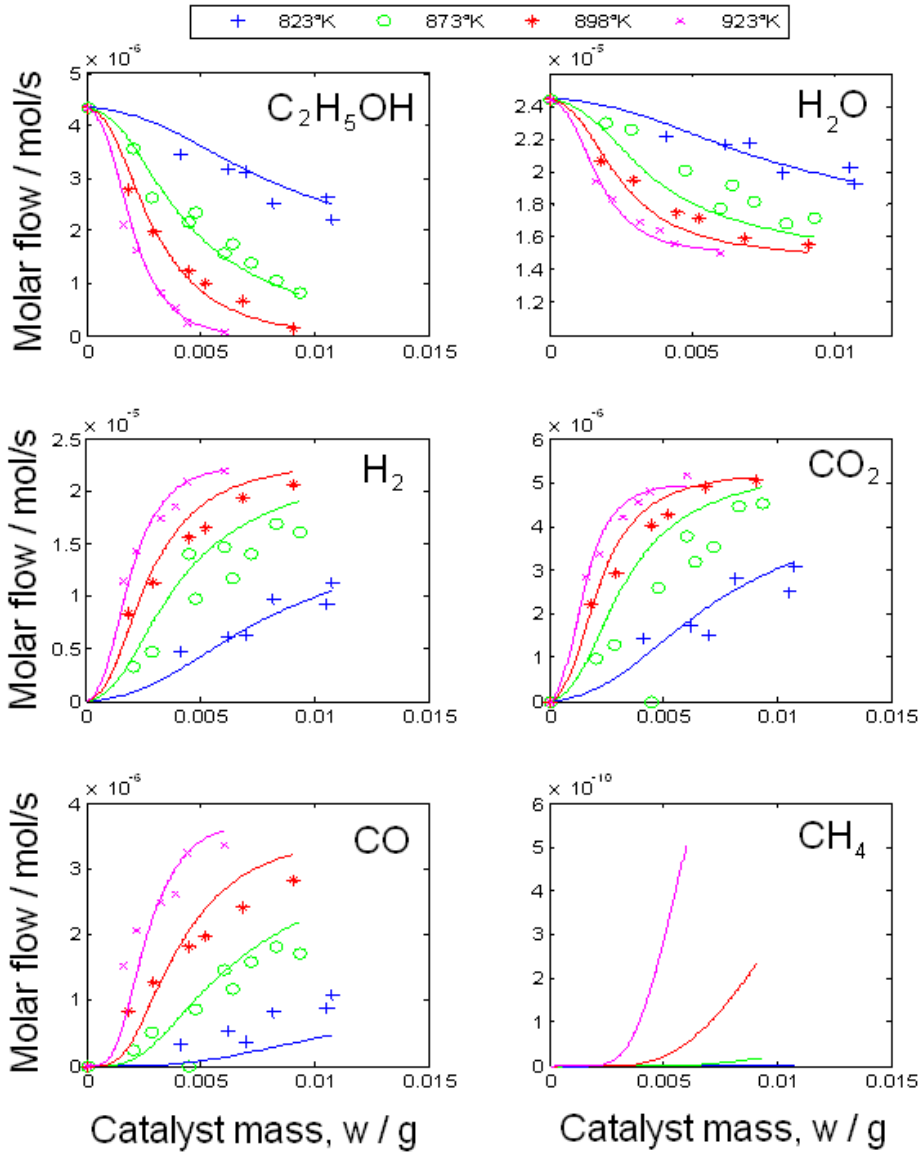

**Fig. 4:** Calculated (continuous line) vs. experimental values reported in Table 1 according to Model 2 (a) and 3 (b) at different temperature.

(a)

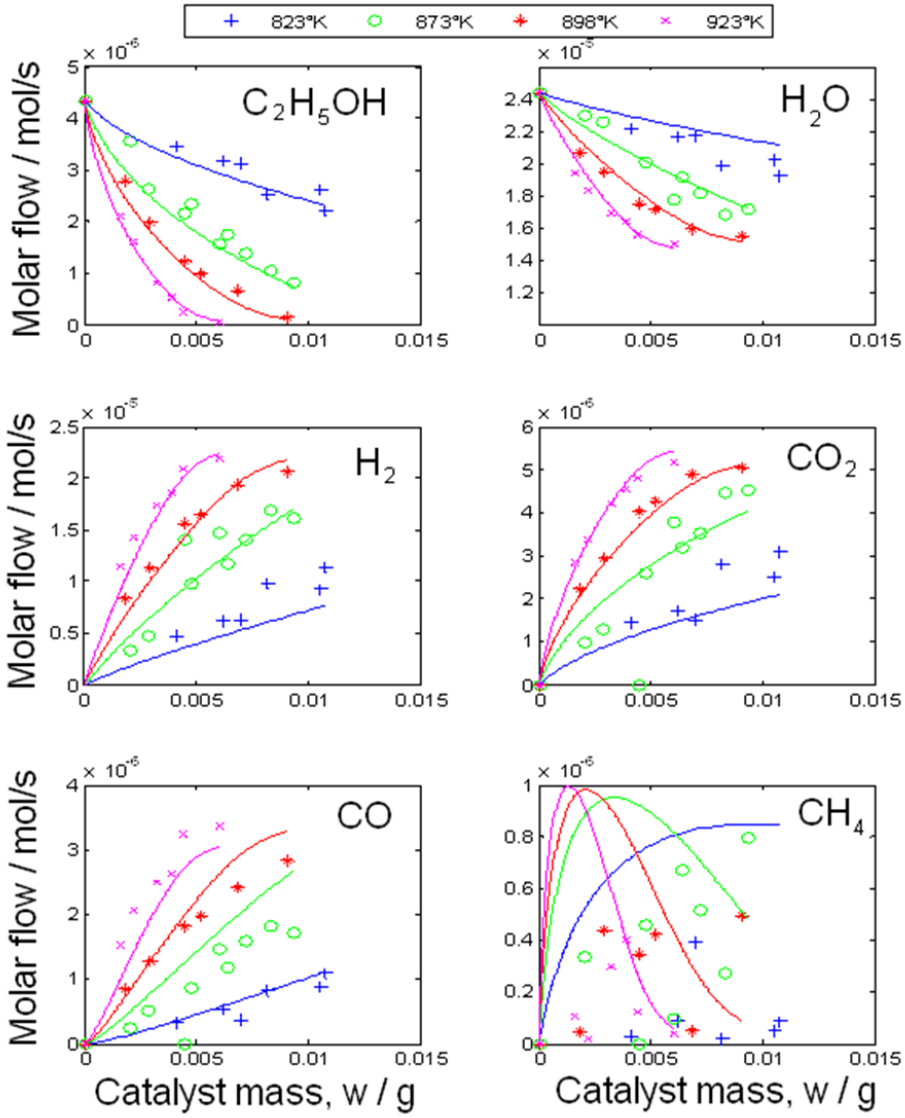

(b)

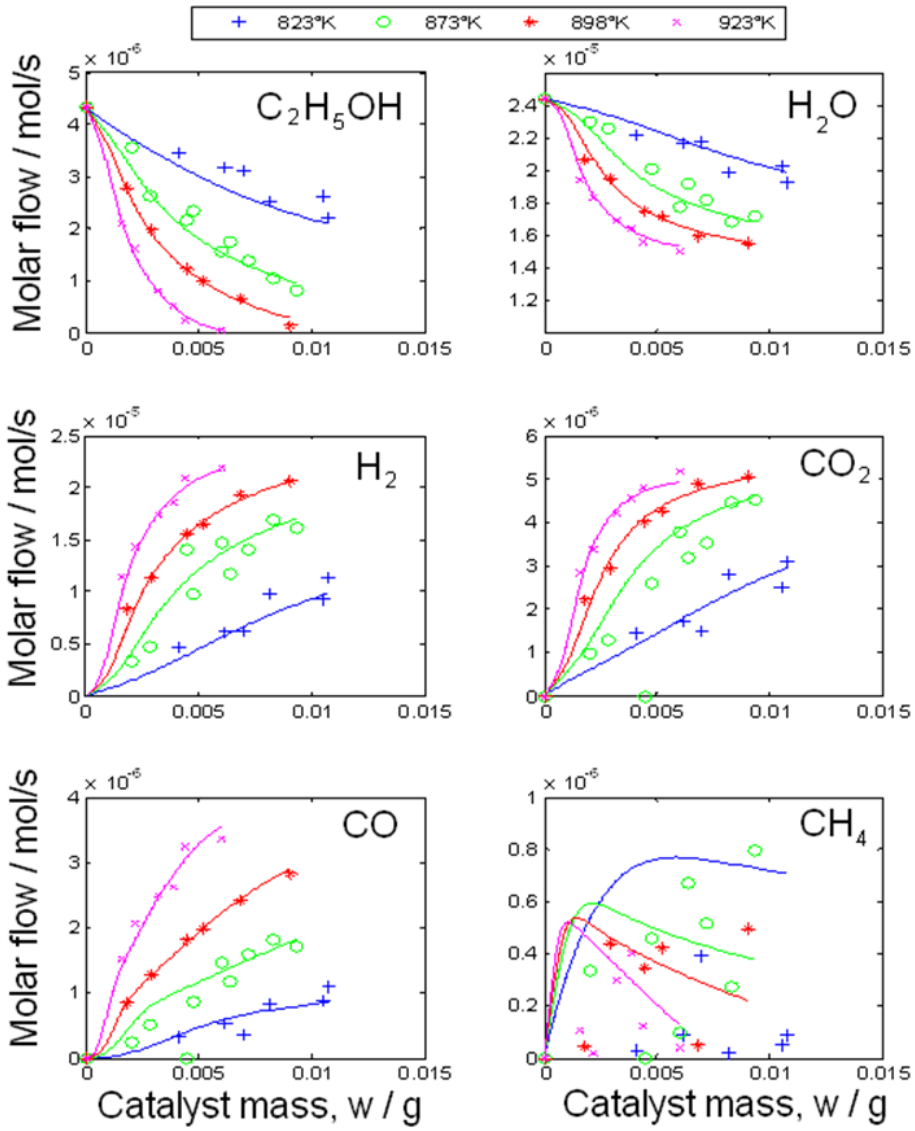
823°K
873°K
898°K
923°K
Molar flow / mol/s
$C_2H_5OH$
$H_2O$
$H_2$
$CO_2$
CO
$CH_4$
Catalyst mass, w / g
Catalyst mass, w / g

**Fig. 5:** Parity plot for Model 3, comparing experimental and calculated outflowing molar flows for each species at variable contact time and reaction temperature. The lines indicate ±10% deviation.